J. Phys.: Condens. Matter **23** (2011) 326005 (8pp) doi:10.1088/0953-8984/23/32/326005

Fe, Mn, and Cr doped $BiCoO_3$ for magnetoelectric application: a first-principles study

Xing-Yuan Chen[1], Ren-Yu Tian[1], Jian-Ming Wu[1], Yu-Jun Zhao[1], Hang-Chen Ding[2] and Chun-Gang Duan[2,3]

[1] Department of Physics and State Key Laboratory of Luminescent Materials and Devices, South China University of Technology, Guangzhou 510640, People's Republic of China
[2] Key Laboratory of Polar Materials and Devices, Ministry of Education, East China Normal University, Shanghai 200241, People's Republic of China
[3] National Laboratory for Infrared Physics, Chinese Academy of Sciences, Shanghai 200083, People's Republic of China

E-mail: zhaoyj@scut.edu.cn, wxbdcg@gmail.com and cgduan@clpm.ecnu.edu.cn

Received 27 April 2011, in final form 23 June 2011
Published 28 July 2011
Online at stacks.iop.org/JPhysCM/23/326005

Abstract

The tetragonal compound $BiCoO_3$ may play a significant role in magnetoelectric devices if its magnetism can be tuned and its strong ferroelectricity maintained. Here we have studied Fe, Mn, and Cr doped $BiCoO_3$ with a concentration of 12.5% by density functional theory (DFT) and DFT + U calculations. It is found that all the doped magnetic ions favor ferromagnetic coupling in the C-type antiferromagnetic $BiCoO_3$ lattice, leading to net magnetic moments of 1, 1, 0 μ_B for $Bi_8Co_7XO_{24}$, where X = Fe, Cr, and Mn, respectively. Meanwhile, the Berry phase calculations indicate that the strong ferroelectricity is almost preserved for Fe, Cr, and Mn doped $BiCoO_3$, with values of 172.7, 152.1, and 169.8 μC cm^{-2}, respectively, close to the original polarization value of 174.9 μC cm^{-2}. As a result, Cr or Fe doping may be useful to make the $BiCoO_3$ system ferrimagnetic while maintaining its excellent ferroelectric performance.

(Some figures in this article are in colour only in the electronic version)

1. Introduction

Multiferroic materials are materials which possess two or more ferroic orderings, e.g., (anti)ferromagnetic, ferroelectric, ferrotoroidic and ferroelastic orderings, in the same phase [1, 2]. As a result, they generally have a spontaneous magnetization which can be switched by an applied magnetic field, or a spontaneous polarization tunable by an applied electric field [3]. More interestingly, couplings between these ferroic orderings offer more degrees of freedom in the design of modern electronic devices [4–8]. Indeed, a number of device applications have been proposed for multiferroic materials, including multi-state memory elements [9, 10], electric field controlled ferromagnetism [11, 12] and magnetic field controlled ferroelectricity [13–15].

In the study of multiferroic materials, special focus has been given to bismuth-based perovskite-structure oxides [16–23], as they generally demonstrate strong ferroelectricity and magnetic orderings at room temperature. Among them, $BiCoO_3$, as a new bismuth-based perovskite-structure oxide with an excellent ferroelectric property, has recently been studied by many groups for its potential application in magnetoelectronic devices [24–30]. Like most other bismuth-based multiferroic materials, however, the magnetic interaction of $BiCoO_3$ is dominated by the short-range antiferromagnetic (AFM) coupling through the superexchange interaction via anions and has no or very weak macroscopic magnetization [31]. A neutron powder diffraction experiment verified that $BiCoO_3$ is a C-type AFM (C-AFM) insulator below the Néel temperature of 470 K [24]. It was also revealed by density functional theory (DFT) calculations that the insulating C-AFM structure is the most stable phase among all the possible spin configurations for the tetragonal phase of $BiCoO_3$ with a large c/a of 1.27 [26].

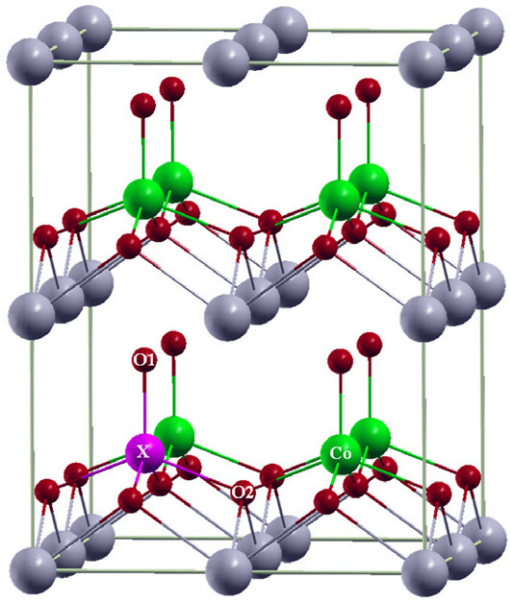

Figure 1. The magnetic impurity doped $2 \times 2 \times 2$ $BiCoO_3$ superlattice with the bismuth, oxygen, cobalt, and impurity ions (X = Fe, Mn, Cr) represented by the gray, red, green, and purple balls, respectively. Two nonequivalent oxygen atoms are marked as O1 and O2.

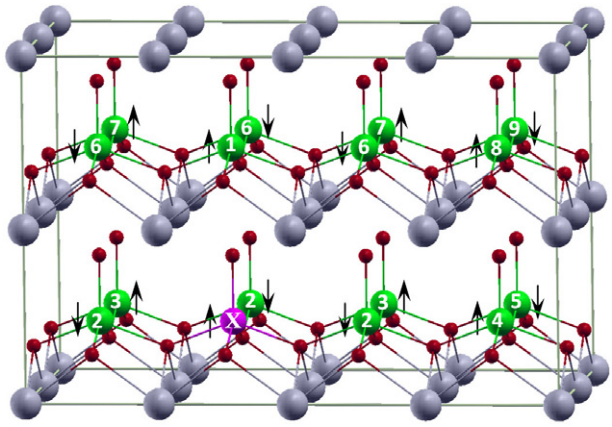

Figure 2. A $4 \times 2 \times 2$ supercell (containing two impurity ions) model to study the favorable coupling between the magnetic impurity ions. With respect to one impurity ion (labeled as X), there are nine nonequivalent positions for the other impurity ion, as labeled from 1 to 9. The arrows indicate the spin directions of these sites under the C-AFM magnetic configuration.

Clearly, $BiCoO_3$ will be of much interest in many multiferroic devices if its magnetic property can be improved. To introduce net magnetic moments in the AFM $BiCoO_3$, a natural choice is to dope magnetic ions with magnetic moments different from that of the Co ions. In fact, Baettig and Spaldin have predicted by *ab initio* calculations that Bi_2FeCrO_6 (BFCO) is a ferrimagnetic and ferroelectric material with a magnetic moment of 2 μ_B/f.u. and a polarization of 80 $\mu C\,cm^{-2}$ [18]. Nechache *et al* reported a saturated magnetization of 20 emu cm^{-3} in their experimental study of epitaxial BFCO thin films [22]. Recently, $BiCr_{0.5}Mn_{0.5}O_3$ has been synthesized at high pressure and high temperature with weak ferromagnetism at low temperatures and showing a giant dielectric constant at room temperature [32]. These studies suggest that it is possible to dope other magnetic ions into the $BiCoO_3$ system.

In this work, we have studied Fe, Mn, and Cr doped $BiCoO_3$ with a concentration of 12.5% through *ab initio* calculations. We find that all the magnetic impurity ions energetically favor ferromagnetic (FM) coupling. In particular, Cr and Fe doping keep the strong ferroelectricity of $BiCoO_3$ while providing net magnetic moments. Mn doping shows weak insulating behavior and provides no macroscopic magnetization. Detailed analysis reveals that interactions between magnetic ions and O ions play critical roles in the multiferroic properties of the doped systems.

2. Computational details

This work was performed by a plane wave method with the interactions between valence electrons and ions represented by the projector augmented wave (PAW) pseudo-potentials as implemented in the Vienna *ab initio* simulation package (VASP) [33]. The generalized gradient approximation (GGA) of the PW91 functional for the exchange and correlation potential was employed [34]. The GGA calculation of transition metal oxides usually leads to a significant underestimation of the band gap. In order to give a better description of the strongly correlated nature of the 3d transition metal ions and obtain more accurate band gaps we therefore adopt the GGA + U method, in which U represents the on-site repulsion energy term originating from the Hubbard model for strongly correlated systems [35]. A $2 \times 2 \times 2$ supercell of $BiCoO_3$, as shown in figure 1, is employed to simulate the magnetic ion (X = Fe, Mn, Cr) doping at a concentration of 12.5%. Here, the doping concentration of 12.5% for the dopants in $BiCoO_3$ is considered since it is expected to be feasible in experiments and the corresponding calculations are affordable. A $6 \times 6 \times 6$ Monkhorst–Pack grid [36] is used for the $2 \times 2 \times 2$ supercell and the energy cutoff is set to as high as 500 eV in the calculations. Meanwhile, a $4 \times 2 \times 2$ superlattice (cf figure 2) is employed to investigate the magnetic coupling between two impurity ions, with a $2 \times 3 \times 3$ Monkhorst–Pack grid [36] and energy cutoff of 400 eV. The large supercells adopted in the calculations allowed us to simulate various distributions of dopants and their magnetic configurations. The convergence criterion for the electronic energy is 10^{-4} eV and the structures are relaxed until the Hellmann–Feynman forces are less than 0.02 eV $Å^{-1}$. The high convergence criterion guaranteed the accuracy of the calculated results. All the structures were fully relaxed.

3. Results and discussion

3.1. Structural properties

The lattice of $BiCoO_3$ has a tetragonal structure (space group $P4mn$), with $a = 3.719$ Å, $c = 4.719$ Å ($c/a = 1.27$) at 5 K determined by the Rietveld method from neutron diffraction

Table 1. Energies of $Bi_8Co_7XO_{24}$ (X = Fe, Mn, Cr) for different magnetic configurations with respect to C-AFM.

	C-AFM	Spin reverse	G-AFM	A-AFM	FM	PM
Fe doped	0	651	158	1018	2457	2277
Mn doped	0	110	125	854	1676	2370
Cr doped	0	273	132	620	1602	2044

data measurement [24]. In this work, various magnetic configurations, including C-AFM, G-AFM, A-AFM, FM, PM, and the spin-reversed configuration have been calculated to explore the most stable states for Fe, Mn, and Cr doped $BiCoO_3$. Here, the C-AFM magnetic configuration means that the AFM coupled *ab* plane is stacked ferromagnetically along the *c* direction; G-AFM stands for the configuration with AFM coupling in all the three directions; the A-AFM magnetic configuration means FM *ab* planes stacked antiferromagnetically along the *c* axis; the spin-reversed configuration means that the spin of the magnetic impurities is reversed with respect to the most stable C-AFM lattice; the PM configuration stands for the paramagnetic state, here approximated by the non-spin-polarized calculation typically employed in first-principles studies. The calculated results are listed in table 1. It is clear from table 1 that all three doped systems have C-AFM as their most stable magnetic configurations. This is because the superexchange interaction is strong in $BiCoO_3$, which is also confirmed by the fact that it requires 0.65, 0.11, and 0.27 eV to reverse the spin orientations of Fe, Mn, and Cr ions in the doped C-AFM $BiCoO_3$, respectively. Our calculated c/a values are 1.29, 1.27, and 1.28 for Fe, Mn, and Cr doped $BiCoO_3$, respectively, very close to that of pure $BiCoO_3$ (i.e. 1.29). Generally, the ferroelectricity is expected to be greater with a larger c/a in a tetragonal perovskite structure [26, 37]. The large values of c/a suggest that Fe, Mn, and Cr doped $BiCoO_3$ may maintain the original strong ferroelectricity. Cai *et al* reported that in pure $BiCoO_3$ hybridizations between Bi–O and Co–O play important roles for the nature of the ferroelectricity and ferromagnetism [26]. Detailed discussions on the impurity ion interaction with the O ion and the spontaneous ferroelectric polarization using the modern polarization theory of Berry phase methods [38] will be presented later.

3.2. Magnetic properties

Although it is confirmed that C-AFM is maintained in the $2 \times 2 \times 2$ supercell of $Bi_8Co_7XO_{24}$, it is still not clear whether the impurity ions could provide net magnetic moments or not. Obviously, the impurity ion provides no net moments when it possesses the same moment as Co as the local magnetic moments of the dopants will be canceled out by the AFM coupled Co ions. Even if the impurity ion possesses a different magnetic moment, it still could not provide a net magnetic moment if the impurity ions themselves favor AFM coupling. This situation was not sufficiently studied in earlier works [18, 21, 22]. Here a $4 \times 2 \times 2$ supercell (cf figure 2) is employed to study the favorable positions of two magnetic impurity ions in the C-AFM magnetic lattice. As shown in figure 2, the additional X impurity ion in the doubled C-AFM magnetic lattice has nine nonequivalent possible positions. Among them, five positions result in FM and four positions result in AFM coupling between the two impurity ions. Our results (shown in table 2) indicate that the magnetic impurity pairs turn out to favor FM coupling, with at least 20, 51, and 41 meV lower energy than that of the most favored AFM configurations for Fe, Mn, and Cr, respectively. Interestingly, the X-3 FM configurations are favored for Fe and Mn doping, while the Cr pair favors the X-8 FM configuration.

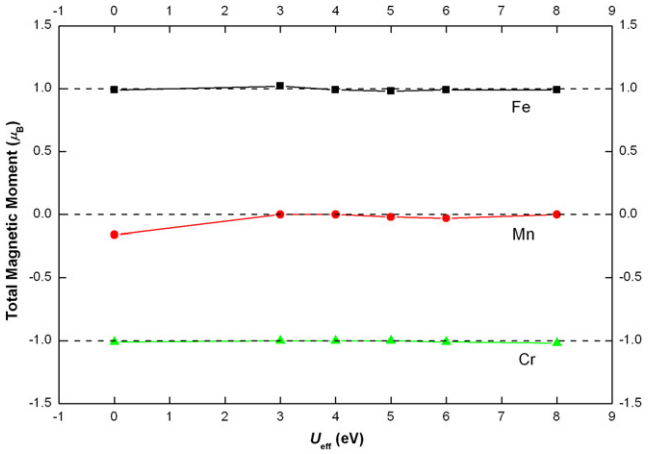

Figure 3. The total magnetic moments of $Bi_8Co_7XO_{24}$ (X = Fe, Mn, Cr) with respect to the U_{eff} values.

Table 2. Total energies (in meV) of nine kinds of nonequivalent magnetic configurations in a supercell of $Bi_{16}Co_{14}X_2O_{48}$ (X = Fe, Mn, Cr), with respect to the energy of their most stable magnetic configuration. Configurations X-1, 3, 4, 7, 8 correspond to FM coupling, and X-2, 5, 6, 9 correspond to AFM coupling.

	FM					AFM			
Config. X-	1	3	4	7	8	2	5	6	9
Fe doped	30	22	7	2	0	20	211	55	252
Mn doped	74	8	8	92	0	88	205	51	226
Cr doped	112	0	256	67	244	41	351	165	258

The above studies confirm the stability of the FM couplings of the impurity ions. As a result, we adopt a $2 \times 2 \times 2$ supercell containing one magnetic impurity ion to study the dependence of the total magnetic moment on the Hubbard U values in the following studies to reduce the computational effort. Here we introduce the GGA+U method by a simplified approach of Dudarev *et al* [39], where the effective Hubbard parameter $U_{eff} = U - J$, with J being the exchange energy. The total magnetic moments of $BiCo_{0.875}X_{0.125}O_3$ (X = Fe, Mn, Cr) with various U_{eff} values are shown in figure 3. It is found that Cr and Fe doping provide a net magnetic moment of 1 μ_B per Fe or Cr in $BiCoO_3$. However, the Mn doping system provides no net magnetic moment.

The above results can be explained by crystal field theory. As we know, the transition metal ions in the B site of the ABO_3 perovskite structure would experience the oxygen octahedral

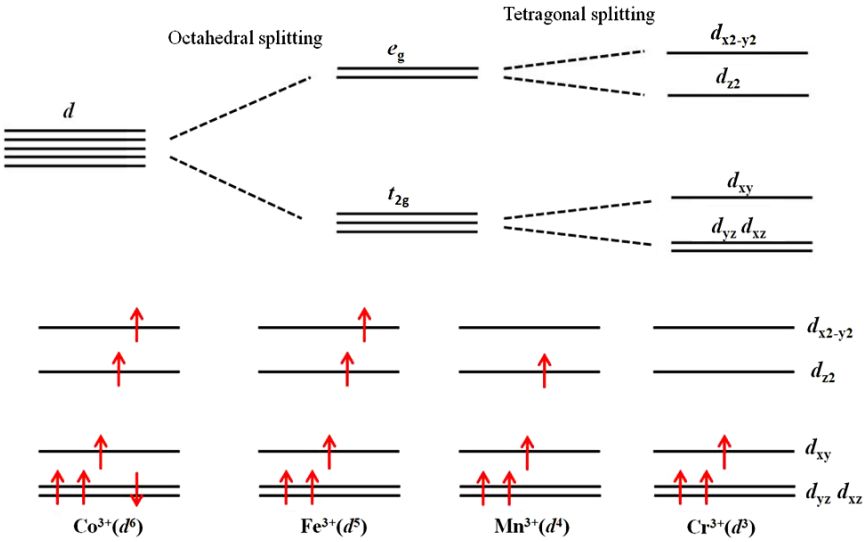

Figure 4. Electronic configuration of 3d levels under octahedral and tetragonal crystal field splitting. The corresponding occupations for 3d electrons of Co^{3+}, Fe^{3+}, Mn^{3+}, and Cr^{3+} are shown with red arrows.

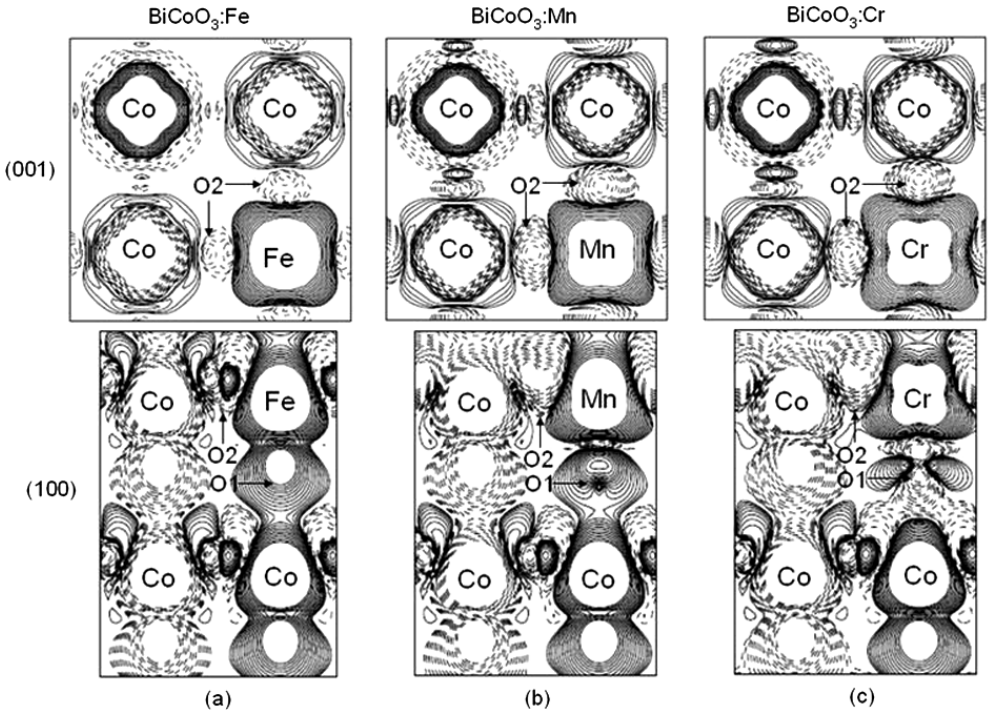

Figure 5. Spin charge density of $BiCoO_3$ on (001) and (100) planes across the impurity ions of (a) Fe, (b) Mn, and (c) Cr, respectively. The spin up and down densities are denoted by solid and dashed lines, respectively. Here the spin density contours start at 0.001 e Å^{-3} and increase successively by a factor of $\sqrt{2}$.

crystal field, which splits the five otherwise degenerate orbital states into t_{2g} and e_g orbital states. The tetragonal symmetry of the current systems will further split these orbital states into $d_{x^2-y^2}$, d_{z^2}, d_{xy} and double degenerate d_{xz} and d_{yz} states, as shown in figure 4. The $Co^{3+}(d^6)$, $Fe^{3+}(d^5)$, $Mn^{3+}(d^4)$, and $Cr^{3+}(d^3)$ ions are expected to possess 4 μ_B, 5 μ_B, 4 μ_B, and 3 μ_B magnetic moment at high spin configuration, respectively. This suggests that the doped Fe(Cr) contributes $1(-1)$ μ_B net magnetic moment while Mn doping provides no net magnetic moment as Mn ion has the same magnetic moment as that of Co ion.

In reality, however, the transition metal ions are not ideal 3^+ ions in the system based on charge transfer analysis, and the interactions between the O ions and magnetic ions play critical roles in the magnetic properties as reflected in the spin charge density plot (see figure 5). The magnetic moments within a

Table 3. The calculated bond lengths between the transition metal (TM) ions and O ions and the corresponding magnetic moments for $U_{\text{eff}} = 4$ eV. O1 and O2 are the apical and planar oxygen atoms, respectively.

		Co–O1	Co–O2	Fe–O1	Fe–O2	Mn–O1	Mn–O2	Cr–O1	Cr–O2
Bond length (Å)		1.78	1.99	1.83	2.00	1.99	1.95	1.90	1.99
Magnetic moment (μ_B)	O	0.30	0.00	0.22	0.00	0.08	−0.10	−0.03	−0.09
	TM	2.95		4.09		3.70		2.85	

sphere of radius 1.302 Å for Co, Fe, Mn, and Cr are close to 3, 4, 4, and 3 μ_B (see table 3), respectively. There are five neighboring O ions to the magnetic ions forming a pyramid structure. The magnetic ions are located at an off center position of the pyramid structure of five O ions. The O ion at the top of the pyramid structure along the [001] direction is denoted as O1, and the other four equivalent O ions are denoted as O2, as indicated in figure 1. As listed in table 3, the magnetic moments of the O1 ions bonded to the impurity Fe, Mn, and Cr ions are 0.22, 0.08, and −0.01 μ_B, respectively, within a sphere of radius of 0.820 Å. The corresponding moments for O2 bonded to Fe, Mn, and Cr ions are 0, −0.10, and −0.09 μ_B, respectively. Here negative moments stand for opposite spins to that of the bonded transition metal ions. The magnetic moments of O1 and O2 around the Co ions are 0.3 and 0 μ_B, respectively. The bond lengths between the magnetic ions and O ions are also listed in table 3, suggesting strong correlation between the bond length and the magnetic moments of the O ions. In the pure $BiCoO_3$, O1 is surrounded by Co ions of nonequivalent distance, while O2 is surrounded by two Co ions of the same distance but inverse spin orientations. As a result, O2 has no net magnetic moment while O1 has a moment of ∼0.3 μ_B in pure $BiCoO_3$. Like the superexchange of Co–O1–Co in pure $BiCoO_3$, Co–O1–Fe superexchange shows strong asymmetry. This introduces 0.22 μ_B magnetic moments at O1 and no remnant magnetic moment for O2. In figure 5, the spin charge density shows an obvious net spin magnetic moment at the O1 ion bonded to the Fe ion and an antisymmetric distribution at the O2 ions bonded to the Fe ion. As a result, the net magnetic moments in the Fe doped system are mainly produced by the difference between the local magnetic moments of the Fe and Co ions. The bond lengths of Mn–O1 and Cr–O1 become longer, and, in particular, the Mn–O1 distance is greater than that of Mn–O2, leading to a significant reduction of the local magnetic moments at O1 bonded to the impurity ions. This enhances the interactions of Mn–O2 and Cr–O2, and therefore increases the net magnetic moments at the O2 ion of reversed spin relative to that of O1. As shown in figure 5, the spin charge densities of the O2 ion bonded to the Mn and Cr ions show remnant magnetic moments, in contrast to the Fe doping case. The changes of local magnetic moments at the O1 and O2 ions bonded to the impurity ions, in fact, reduce the total moments in the spin direction of the impurity ions. As a consequence, the Mn doping system provides no remnant magnetic moment despite a difference of around 1 μ_B local magnetic moment between Mn and Co ions, while Cr doping induces −1 μ_B net magnetic moment although the local moment of the Cr ion is nearly the same as that of Co.

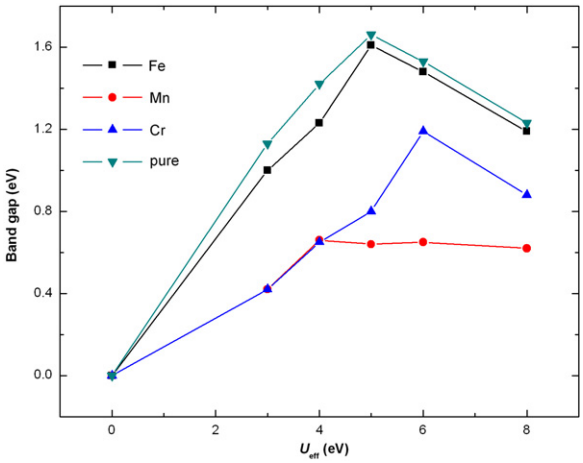

Figure 6. The calculated band gaps with respect to the adopted U_{eff} values for pure and Fe, Mn, and Cr doped $BiCoO_3$.

3.3. Ferroelectric and insulating properties

Ferroelectric materials must be insulators. Indeed, the greater the energy gap of the ferroelectric, the less electric leakage during the ferroelectric switching process is expected. Doping magnetic impurities in Bi-based perovskites, however, generally degrades the insulating behavior and thus the ferroelectricity of the materials. Therefore, it is instructive to study the band gap of the doped $BiCoO_3$. For the reason mentioned before, we perform additional electronic structure calculations with the GGA + U method. As a qualitative investigation, we employed the same U_{eff} values for the Co, Fe, Mn, and Cr elements with a series of values 0, 3, 4, 5, 6, 8 eV in the additional electronic structure calculations. We have listed the band gaps of $BiCo_{0.875}X_{0.125}O_3$ (X = Fe, Mn, Cr) with respect to the Hubbard U_{eff} in figure 6. When $U_{\text{eff}} = 0$, we find no band gaps in any of the systems. Only when the Hubbard U_{eff} is turned on can the band gaps appear. This, again, shows the importance of taking into account the on-site Coulomb repulsion effect. Of all the doped situations, we find that the Fe doping systems have the largest band gaps within the GGA+U framework. The band gap of Fe doped system increases from 0 to 1.61 eV as the value of U_{eff} changes from 0 to 5 eV, while it becomes narrower with increasing values of U_{eff} beyond 6 eV. The situations are similar in the Mn and Cr doped systems, where their largest band gaps (0.66 eV for Mn and 1.19 eV for Cr) emerge at $U_{\text{eff}} = 4$ eV and $U_{\text{eff}} = 6$ eV, respectively. The relative values of the band gaps follow the series of pure $BiCO_3$ > $BiCoO_3$: Fe > $BiCoO_3$: Cr > $BiCoO_3$: Mn, independent of the U_{eff} values.

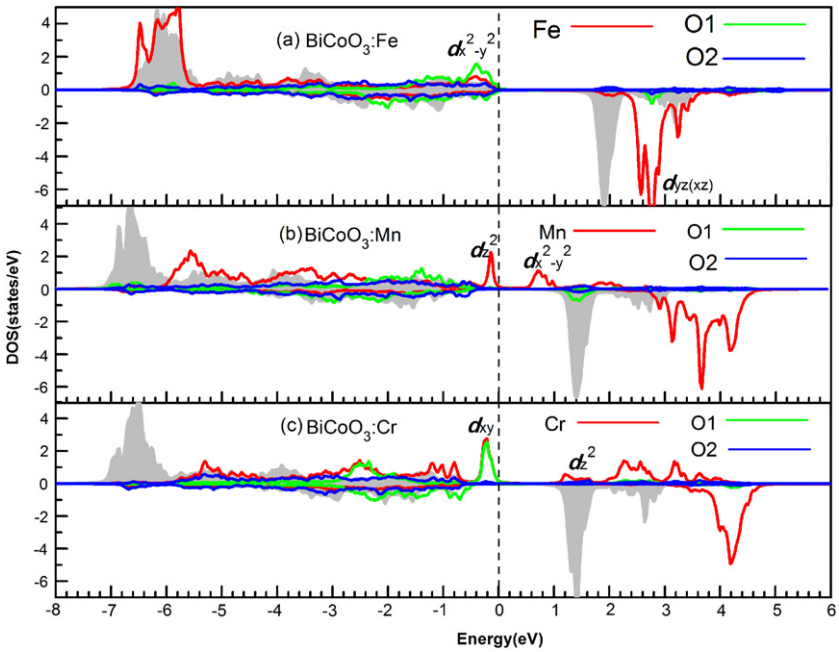

Figure 7. The projected DOS of (a) Fe, (b) Mn, and (c) Cr doped $BiCoO_3$ corresponding to $U_{\text{eff}} = 4$ eV, where the VBM is set to 0 and the spin up and down plots are denoted by positive and negative values, respectively. The shaded plots correspond to the Co ion.

The change of the energy gap with different doping ions can be explained by projected density of states (DOS) analysis. As we know, the valence band maximum (VBM) and the conduction band minimum (CBM) of the ferroelectric phase of tetragonal ABO_3 perovskite are generally determined by the electronic states of the B atom and the bonded O atoms. From figure 7, which shows the projected DOS of doped $BiCoO_3$ with $U_{\text{eff}} = 4$ eV, we can see that the energy levels of the occupied 3d states of the dopants and the Co ion are in the series Cr > Mn > Fe > Co. Therefore the VBM region is dominated by the occupied 3d states of the doping ions, which are hybridized with O1 atoms to some extent. As the occupied Fe 3d states have slightly higher energy than that of the Co ions, the gap in the Fe doped system is thus determined by the occupied Fe 3d states and the unoccupied Co 3d states. Therefore, the energy gap of the Fe doped system is just a little bit smaller than that of the pure $BiCoO_3$ system. Noticing that the unoccupied 3d states of both the Fe and Co ions are actually spin down states, we see that the gaps are indeed opened by the on-site Coulomb repulsion effect. The situations for Cr and Mn doped systems, however, are quite different, since the 3d states of these ions are less than half filled. For Cr ions, the energy level of the unoccupied d_{z^2} state is about 1.2 eV above the Fermi level, which is similar to that of the lowest unoccupied 3d state of the Co atom. For Mn atoms, the unoccupied $d_{x^2-y^2}$ state is only about 0.6 eV above the Fermi level, much lower than that of the lowest unoccupied Co 3d state. The energy gap of the Mn doped system is then determined by the occupied and unoccupied Mn 3d states. This also explains why the energy gaps of the Mn doped system are not sensitive to the Hubbard U_{eff} after $U_{\text{eff}} > 4$ eV.

The spontaneous ferroelectric polarizations of $BiCo_{0.875}X_{0.125}O_3$ (X = Fe, Mn, Cr) have been calculated by the Berry phase method [38]. The results indicate that the spontaneous ferroelectric polarization of pure $BiCoO_3$ and $BiCo_{0.875}X_{0.125}O_3$ (X = Fe, Mn, Cr) are 174.9, 172.7, 152.1, and 169.8 μC cm^{-2}, respectively. The spontaneous ferroelectric polarization directions of the pure and doped systems are all nearly along the [001] direction, and the calculated values have no apparent dependence on the employed Hubbard U_{eff} values as the structures have no significant changes as long as the energy gap is opened. Note that our calculated ferroelectric polarization of pure $BiCoO_3$ (174.9 μC cm^{-2}) is in excellent agreement with earlier works [22, 25]. We find that the decrease of the ferroelectric polarizations of the doped system can be roughly attributed to the smaller ferroelectric polarizations of the bulk $BiXO_3$ (X = Fe, Mn, Cr) system, with the values of 155.7, 117.3, and 90.0 μC cm^{-2}, respectively. The fact that the Mn doped system has a smaller ferroelectric polarization than that of the Cr doped system might be caused by the much weaker hybridization between the Mn and O1 ions, as is clearly shown in figure 7. This is also confirmed by Born effective charge (BEC) analysis [40]. The BEC of Mn (3.12) in the doped system is smaller than that of Cr (3.27), whereas the displacements between Mn/Cr and the O2 plane (0.58/0.57 Å) are nearly the same. This explains why the polarization of Mn doping is smaller than that of Cr doping.

4. Conclusion

In summary, our theoretical study indicates that doped Cr and Fe ions could be FM ordered in $BiCoO_3$ and provide a net magnetic moment of 1 μ_B per impurity in $BiCoO_3$, while the Mn doped system does not provide macroscopic

magnetization. The magnetism of the Mn, Fe, and Cr doped $BiCoO_3$ is explained with a simple crystal field theory, as well as local interactions between the oxygen ions and the magnetic cations. Meanwhile, Berry phase calculations demonstrate that the strong ferroelectricity of pure $BiCoO_3$ is almost maintained in these doped systems. The potential use of Fe and Cr doped $BiCoO_3$ in magnetoelectric applications is suggested by their confirmed macroscopic magnetism and strong ferroelectricity.

Acknowledgments

We are grateful for the computer time at the High Performance Computer Center of Shenzhen Institute of Advanced Technology (SIAT), Chinese Academy of Science. This work was supported by NSFC (Grant Nos 10704025, 50771072, 50832003), PCSIRT, NCET-08-0202, Education Foundation of Science and Technology Innovation of the Ministry of Education, China (Grant No. 708070), and the Fundamental Research Funds for the Central Universities, SCUT, 2009ZZ0068/2009ZM0165.

References

[1] Schmid H 1994 Multi-ferroic magnetoelectrics *Ferroelectrics* **162** 317
[2] Picozzi S and Ederer C 2009 First principles studies of multiferroic materials *J. Phys.: Condens. Matter* **21** 303201
[3] Wood V E and Austin A E 1975 *Magnetoelectric Interaction Phenomena in Crystals* ed A J Freeman and H Schmid (New York: Gordon and Breach)
[4] Fiebig M 2005 Revival of the magnetoelectric effect *J. Phys. D: Appl. Phys.* **38** R123
[5] Spaldin N A and Fiebig M 2005 The renaissance of magnetoelectric multiferroics *Science* **309** 391
[6] Eerenstein W, Mathur N D and Scott J F 2006 Multiferroic and magnetoelectric materials *Nature* **442** 759
[7] Ramesh R and Spaldin N A 2007 Multiferroics: progress and prospects in thin films *Nature Mater.* **6** 21
[8] Wang K F, Liu J M and Ren Z F 2009 Multiferroicity: the coupling between magnetic and polarization orders *Adv. Phys.* **58** 321
[9] Gajek M, Bibes M, Fusil S, Bouzehouane K, Fontcuberta J, Barthelemy A E and Fert A 2007 Tunnel junctions with multiferroic barriers *Nature Mater.* **6** 296
[10] Velev J P, Duan C G, Burton J D, Smogunov A, Niranjan M K, Tosatti E, Jaswal S S and Tsymbal E Y 2009 Magnetic tunnel junctions with ferroelectric barriers: prediction of four resistance states from first principles *Nano Lett.* **9** 427
[11] Duan C-G, Jaswal S S and Tsymbal E Y 2006 Predicted magnetoelectric effect in Fe/$BaTiO_3$ multilayers: ferroelectric control of magnetism *Phys. Rev. Lett.* **97** 047201
[12] Chu Y H *et al* 2008 Electric-field control of local ferromagnetism using a magnetoelectric multiferroic *Nature Mater.* **7** 478
[13] Kimura T, Goto T, Shintani H, Ishizaka K, Arima T and Tokura Y 2003 Magnetic control of ferroelectric polarization *Nature* **425** 551
[14] Lottermoser T, Lonkai T, Amann U, Hohlwein D, Ihringer J and Fiebig M 2004 Magnetic phase control by an electric field *Nature* **430** 541
[15] Nan C W, Bichurin M I, Dong S X, Viehland D and Srinivasan G 2008 Multiferroic magnetoelectric composites: historical perspective, status, and future directions *J. Appl. Phys.* **103** 031101
[16] Hill N A, Battig P and Daul C 2002 First principles search for multiferroism in $BiCrO_3$ *J. Phys. Chem.* B **106** 3383
[17] Niitaka S, Azuma M, Takano M, Nishibori E, Takata M and Sakata M 2004 Crystal structure and dielectric and magnetic properties of $BiCrO_3$ as a ferroelectromagnet *Solid State Ion.* **172** 557
[18] Baettig P and Spaldin N A 2005 *Ab initio* prediction of a multiferroic with large polarization and magnetization *Appl. Phys. Lett.* **86** 012505
[19] Ederer C and Spaldin N A 2005 Weak ferromagnetism and magnetoelectric coupling in bismuth ferrite *Phys. Rev.* B **71** 60401
[20] Feiming B, Junling W, Wuttig M, JieFang L, Naigang W, Pyatakov A P, Zvezdin A K, Cross L E and Viehland D 2005 Destruction of spin cycloid in $(111)_c$-oriented $BiFeO_3$ thin films by epitiaxial constraint: enhanced polarization and release of latent magnetization *Appl. Phys. Lett.* **86** 32511
[21] Baettig P, Ederer C and Spaldin N A 2005 First principles study of the multiferroics $BiFeO_3$, Bi_2FeCrO_6, and $BiCrO_3$: structure, polarization, and magnetic ordering temperature *Phys. Rev.* B **72** 214105
[22] Nechache R, Harnagea C, Pignolet A, Normandin F, Veres T, Carignan L P and Menard D 2006 Growth, structure, and properties of epitaxial thin films of first-principles predicted multiferroic Bi_2FeCrO_6 *Appl. Phys. Lett.* **89** 102902
[23] Suchomel M R, Thomas C I, Allix M, Rosseinsky M J, Fogg A M and Thomas M F 2007 High pressure bulk synthesis and characterization of the predicted multiferroic $Bi(Fe_{1/2}Cr_{12})O_3$ *Appl. Phys. Lett.* **90** 112909
[24] Uratani Y, Shishidou T, Ishii F and Oguchi T 2005 First-principles predictions of giant electric polarization *Japan. J. Appl. Phys.* **44** 7130
[25] Belik A A *et al* 2006 Neutron powder diffraction study on the crystal and magnetic structures of $BiCoO_3$ *Chem. Mater.* **18** 798
[26] Cai M Q, Liu J C, Yang G W, Cao Y L, Tan X, Chen X Y, Wang Y G, Wang L L and Hu W Y 2007 First-principles study of structural, electronic, and multiferroic properties in $BiCoO_3$ *J. Chem. Phys.* **126** 154708
[27] Ravindran P, Vidya R, Eriksson O and Fjellvag H 2008 Magnetic-instability-induced giant magnetoelectric coupling *Adv. Mater.* **20** 1353
[28] Ming X, Meng X, Hu F, Wang C Z, Huang Z F, Fan H G and Chen G 2009 Pressure-induced magnetic moment collapse and insulator-to-semimetal transition in $BiCoO_3$ *J. Phys.: Condens. Matter* **21** 295902
[29] Oka K *et al* 2010 Pressure-induced spin-state transition in $BiCoO_3$ *J. Am. Chem. Soc.* **132** 9438
[30] Uratani Y, Shishidou T and Oguchi T 2009 First-principles study on the magnetic anisotropy in multiferroic $PbVO_3$ and $BiCoO_3$ *J. Phys. Soc. Japan* **78** 084709
[31] Hill N A 2000 Why are there so few magnetic ferroelectrics? *J. Phys. Chem.* B **104** 6694
[32] Mandal P, Iyo A, Tanaka Y, Sundaresan A and Rao C N R 2010 Structure, magnetism and giant dielectric constant of $BiCr_{0.5}Mn_{0.5}O_3$ synthesized at high pressures *J. Mater. Chem.* **20** 1646
[33] Kresse G and Furthmüller J 1996 Efficiency of *ab initio* total energy calculations for metals and semiconductors using a plane-wave basis set *Comput. Mater. Sci.* **6** 15
Kresse G and Joubert D 1999 From ultrasoft pseudopotentials to the projector augmented-wave method *Phys. Rev.* B **59** 1758
[34] Perdew J P and Wang Y 1992 Accurate and simple analytic representation of the electron–gas correlation energy *Phys. Rev.* B **45** 13244

[35] Liechtenstein A I, Anisimov V I and Zaanen J 1995 Density-functional theory and strong interactions: orbital ordering in Mott–Hubbard insulators *Phys. Rev.* B **52** R5467
[36] Monkhorst H J and Pack J D 1976 Special points for Brillouin-zone integrations *Phys. Rev.* B **13** 5188–93
[37] Kan E, Xiang H J, Lee C, Wu F, Yang J L and Whangbo M H 2010 Ferroelectricity in perovskites with s^0 A-site cations: toward near-room-temperature multiferroics *Angew. Chem. Int. Edn Engl.* **49** 1603
[38] Kingsmith R D and Vanderbilt D 1993 Theory of polarization of crystalline solids *Phys. Rev.* B **47** 1651
[39] Dudarev S L, Botton G A, Savrasov S Y, Humphreys C J and Sutton A P 1998 Electron-energy-loss spectra and the structural stability of nickel oxide: an LSDA + U study *Phys. Rev.* B **57** 1505
[40] Pick R M, Cohen M H and Martin R M 1970 Microscopic theory of force constants in the adiabatic approximation *Phys. Rev.* B **1** 910